Nucleic Acids Research, 2017 **1**
doi: 10.1093/nar/gkx498

Determining the folding and binding free energy of DNA-based nanodevices and nanoswitches using urea titration curves

Andrea Idili[1], Francesco Ricci[1,*] and Alexis Vallée-Bélisle[2,*]

[1]Chemistry Department, University of Rome Tor Vergata, Rome 00133, Italy and [2]Laboratory of Biosensors and Nanomachines, Département de Chimie, Université de Montréal, Montreal, Québec H3T-1J4, Canada

Received February 20, 2017; Revised May 23, 2017; Editorial Decision May 25, 2017; Accepted May 27, 2017

ABSTRACT

DNA nanotechnology takes advantage of the predictability of DNA interactions to build complex DNA-based functional nanoscale structures. However, when DNA functional and responsive units that are based on non-canonical DNA interactions are employed it becomes quite challenging to predict, understand and control their thermodynamics. In response to this limitation, here we demonstrate the use of isothermal urea titration experiments to estimate the free energy involved in a set of DNA-based systems ranging from unimolecular DNA-based nanoswitches to more complex DNA folds (e.g. aptamers) and nanodevices. We propose here a set of fitting equations that allow to analyze the urea titration curves of these DNA responsive units based on Watson–Crick and non-canonical interactions (stem-loop, G-quadruplex, triplex structures) and to correctly estimate their relative folding and binding free energy values under different experimental conditions. The results described herein will pave the way toward the use of urea titration experiments in the field of DNA nanotechnology to achieve easier and more reliable thermodynamic characterization of DNA-based functional responsive units. More generally, our results will be of general utility to characterize other complex supramolecular systems based on different biopolymers.

INTRODUCTION

Over the last 10 years, DNA nanotechnology has demonstrated how synthetic nucleic acid strands can be employed to design and engineer nanoscale structural and functional systems of increasing complexity (1–3). With its highly predictable interactions and thermodynamics, DNA can in fact be considered as the biomaterial of choice to develop precise spatio-temporally controlled nanostructures (4,5) and to engineer supramolecular systems with functions ranging from sensing (6,7) to computing (8,9), molecular transport (10,11) and catalysis (12,13). In order to design such DNA-based systems, user-friendly softwares such as Mfold (14), NUPACK (15) and IDT SciTools (16), which allow to quantitatively predict the free energy of Watson–Crick interactions, are increasingly employed. A main limitation of these prediction tools, however, is that they inevitably fail to predict energies of more complex DNA tertiary structures (i.e. triplex, i-motif, G-quadruplex, aptamers, DNAzymes) based on non-canonical interactions. They also do not predict the effect of chemical modifications such as the addition of labeling molecules (e.g. fluorophores, quenchers, etc.) or the use of modified nucleotides (17–19).

To overcome these limitations, several experimental approaches have been employed in recent years to estimate the free energy of DNA-based systems. These include melting curves, isothermal titration calorimetry and titration binding curves (20–22). Unfortunately, these approaches typically suffer from considerable drawbacks, which include low sensitivity and high cost (calorimetry), lack of structural information (melting curves) and inability to measure binding free energies of high-affinity interactions (i.e. K_D below pM) (binding curves). Over the last three decades, urea chemical denaturation (23–28) has become the method of choice to evaluate the free energy of proteins and other biopolymers (23–25). Such method was also found of utility, although with limited examples, in the characterization of ribozyme and RNA structural folding (26–28). Despite its relative simplicity and precise free energy measurements, however, urea titration experiments have seen little (29,30), if any application in the field of DNA-based supramolecular chemistry. Motivated by this, here we demonstrate the applicability of urea titration experiments to determine the folding and binding free energy of a set of DNA responsive units (Figure 1) based on Watson–Crick and non-canonical interactions.

*To whom correspondence should be addressed. Francesco Ricci. Tel: +39 06 7259 4422; Fax: +39 06 72594328; Email: francesco.ricci@uniroma2.it
Correspondence may also be addressed to Alexis Vallée-Bélisle. Tel: +1 514 343 6219; Email: a.vallee-belisle@umontreal.ca

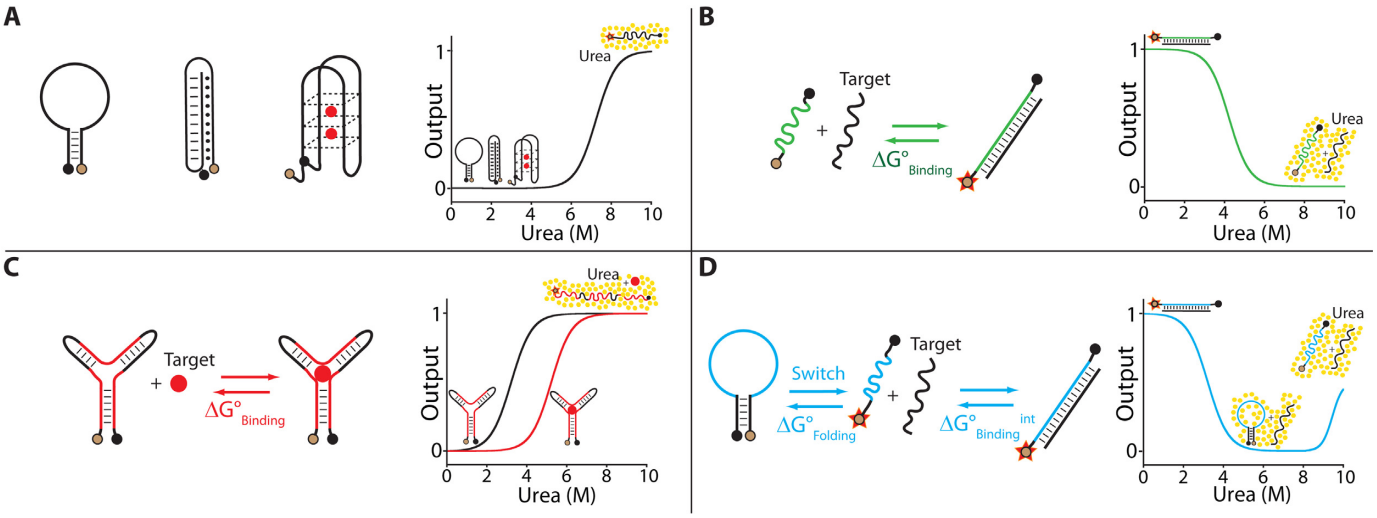

Figure 1. Determining the thermodynamics of DNA-based nanosystems using urea titration curves. (**A**) Folding free energies of DNA unimolecular structures. (**B**) Binding free energies of DNA–DNA complexes. (**C**) Binding free energies between a DNA aptamer and its non-DNA target. (**D**) Binding free energies between a DNA conformational nanoswitch and its DNA target.

MATERIALS AND METHODS

Oligonucleotides

All oligonucleotides employed in this work were synthesized, labeled and purified (HPLC and reverse phase) by IBA GmBH (Göttingen, Germany) or DNA Technology (Risskov, Denmark) and used without further purification. Unless otherwise stated the labeled oligonucleotides were dissolved in Millipore water at a concentration of 1 mM while the non-labeled oligonucleotide were dissolved in the relevant buffer (100 mM Tris buffer, 10 mM $MgCl_2$, pH 7.8) at a concentration of 100 μM. The final concentration of the oligonucleotides was confirmed using Tecan Infinite M200pro (Männedorf, Switzerland) through NanoQuant Plate™. Before use, each oligonucleotide solution was heated to 95°C for 5 min and then allowed to cool to room temperature for 2 h. The sequences of the labeled and unlabeled oligonucleotides used in this work are given below.

Labeled oligonucleotides

In this work we used a set of four unimolecular nanoswitches that form stem-loop structures as shown in Figures 1A, 2A and Supplementary Figure S1. These are labeled with 6-carboxyfluorescein (6-FAM) and Black Hole Quencher 1 (BHQ-1) at the 5' and 3' ends, respectively with the following sequences:

Variant 1GC: 5'-(6-FAM)-AATCAT**CCCCCCTTTTCTTTT**ATGATG-(BHQ-1)-3'

Variant 2GC: 5'-(6-FAM)-ACTCAT**CCCCCCTTTTCTTTT**ATGAGG-(BHQ-1)-3'

Variant 3GC: 5'-(6-FAM)-ACTCAC**CCCCCCTTTTCTTTT**GTGAGG-(BHQ-1)-3'

Variant 4GC: 5'-(6-FAM)-ACTCGC**CCCCCCTTTTCTTTT**GCGAGG-(BHQ-1)-3'

For all the sequences above the nucleotides in bold represent the portion complementary to a 15-nt DNA strand (called target) and the underlined nucleotides represent the self-complementary stem portion. All variants present an additional adenine nucleotide, after the 6-FAM and guanine nucleotide, before the BHQ-1.

The unimolecular nanoswitch that folds into a G-quadruplex structure in Figures 1A and 2C, is labeled with a 6-FAM at the 5' end and a BHQ-1 at the 3' end following this sequence:

G-quadruplex: 5′-(6-FAM)-TTGGGTTAGGGTTAGGGTTAGGGTT-(BHQ-1)-3′

The two unimolecular nanoswitches that fold into unimolecular triplex structures in Figures 1A and 2D, are labeled with a Black Hole Quencher 2 (BHQ-2) at position 13 (modified T-nucleotide) and with an Alexafluor 680 (AF680) at the 3'end are:

80% TAT: 5'-AAGAA-AAGAA-**TTT**(BHQ-2)**A**-TTCTT-TTCTT-CTTTG-TTCTT-TTCTT- (AF680)-3'

100% TAT: 5'-AAAAA-AAAAA-**TTT**(BHQ-2)**A**-TTTTT-TTTTT-CTTTG-TTTTT-TTTTT- (AF680)-3'

In the above sequences, the nucleotides in bold represent the loop of the duplex portion and the underlined nucleotides represent the loop for the parallel triplex region (Supplementary Figure S2).

The duplex probes used as controls were labeled with BHQ-2 at the 5' end and at the 3'end with AF680. The sequences of the control duplex probes were as follows:

Control duplex 80% TA:

5'-(BHQ-2) AAGAA-AAGAA-**CTTG**-TTCTT-TTCTT (AF680)-3'

Control duplex 100% TA:

5'-(BHQ-2) AAAAA-AAAAA-**CTTG**-TTTTT-TTTTT (AF680)-3'

For all the sequences above the bases in bold represent the loop portion.

The sequence of the 17-nt linear strand (Figure 1B) is labeled with a 6-FAM at the 5' end and a BHQ-1 at the 3' end:

Linear DNA: 5'-(6-FAM)-A-**CCCCCCTTTTCTTTT**-G-(BHQ-1)-3'

The nucleotides in bold represent the portion complementary to the DNA target strand. This sequence also contains an additional adenine nucleotide, after the 6-FAM and guanine nucleotide, before the BHQ-1.

Finally, the cocaine-binding aptamer in Figures 1C and 4 is a 38-nt DNA strand labeled with 6-FAM at the 5' end and BHQ-1 at the 3'end:

Cocaine aptamer: 5'(6-FAM)-GGGAGACAAGGAAA ATCCTTCAATGAAGTGGGTCGA CA(BHQ-1)-3'

Non-labeled oligonucleotides

The following DNA sequences were used as targets of both the stem-loop and linear strand labeled oligonucleotides described above:

15-nt: 5'-AAAAGAAAAGGGGGG-3'
14-nt: 5'- AAAAGAAAAGGGGG-3'
13-nt: 5'- AAAAGAAAAGGGG-3'
12-nt: 5'- AAAAGAAAAGGG-3'
11-nt: 5'- AAAAGAAAAGG-3'

Urea titration curves

Urea titration curves were obtained by starting from a solution (800 μl) containing the studied DNA-based system and by sequentially increasing the urea concentration by adding increasing volumes of a 10 M urea solution prepared in the working buffer solution and containing the same concentration of the investigated DNA-based system (to avoid change in the concentration of the studied DNA-based system and in ionic strenght). For each urea concentration the system was allowed to equilibrate for 2 min prior to measurement. The fluorescence equilibrated values were obtained using a Cary Eclipse Fluorimeter (Agilent Technologies) and fitted using the relevant Equations (1, 2 and 4). We note that it is also possible to perform the experiment in the opposite direction (from 10 M to 0 M urea) (see Supplementary Figure S3). The reported urea titration curves have been normalized through the use of the interpolation model (23).

Thermal melting curves

Thermal melting curves were obtained using a Cary Eclipse Fluorimeter (Agilent Technologies), and a total reaction volume of 800 μl. The melting curves were performed in the indicated buffer at a concentration of 10 nM (for stem-loop switches) and 100 nM (for unimolecular triplex and G-quadruplex switches). Before the experiment the oligos were heated to 95°C for 5 min and then allowed to cool to room temperature for 1 h. Melting curves were performed by heating from 20 to 95°C at a rate of $1°C{\cdot}min^{-1}$ and the reported melting curves have been normalized through the use of the interpolation model (20,45) and the data analyzed as reported elsewhere (20,45).

Binding curves

Binding curves were obtained using a fixed concentration of the relevant DNA probe and by adding increasing concentrations of the relevant target in a 800 μl volume cuvette. The fluorescence measurements were obtained using a Cary Eclipse Fluorimeter (Agilent Technologies) with excitation at 495 (±5) nm and acquisition between 510 and 530 nm. The fluorescence signals at each target concentration were recorded every 10 min until they reached the equilibrium. The equilibrated values were fitted to a single-site binding mechanism ($[X]$ = target concentration; F_B = fluorescence in the presence of saturating concentration of target; $F_{[T]}$ = fluorescence in the presence of different concentration of target; F_0 = background fluorescence; $[P]$ = concentration of the probe or switch; K_D = dissociation constant):

$$F_{[T]} = F_0 - \left(\frac{[P]+[X]+K_D-\sqrt{([P]+[X]+K_D)^2-4*[P]+[X]}}{2*[P]}\right)*(F_0-F_B)$$

Nupack simulations

We used NUPACK (http://www.nupack.org/) to predict the folding and binding free energies of the DNA systems (15). The DNA sequences in presence or in absence of complementary DNA target were analyzed by the software using the following parameters: (i) temperature: 25 or 37°C; (ii) number of strand species: 1 (for folding free energy) or 2 (for binding free energy); (iii) maximum complex size: 4; in advanced options; (iv) $[Na^+] = 0.1$ M, $[Mg^{++}] = 0.01$ M; (v) dangle treatment: all.

Further experimental details, fitting protocols, reagents and DNA sequences are given in the Supplementary Data.

RESULTS

Determining folding free energies of DNA unimolecular structures

Urea titration curves can be employed to determine the folding free energy of unimolecular DNA structures (Figure 1A). We first determine the folding free energy of a simple DNA secondary structure solely based on Watson–Crick interactions. To do so, we employed a DNA strand with self-complementary ends that folds into a stem-loop structure. This structure has been widely exploited in structure-switching DNA-based sensors (31,32), nanomachines (33,34) and synthetic biology (35). We designed four stem-loop variants that retain a common loop sequence but differ in their stem sequence (Supplementary Figure S1). Specifically, we used a stem of 5 nt and modulated its stability by gradually changing the GC/AT content. In order to monitor the unfolding transition of these DNA folds, we labeled them with a fluorophore (6-FAM) and a quencher (BHQ-1) at the two ends (5' and 3', respectively). The urea titration curves of all four stem-loop variants reveal a single unfolding transition as shown in Figure 2A. These curves (fluorescence (F) versus urea concentration, [U]) were fitted by using a classic two-state denaturation model, Equation (1) (SI Section 5), (23,36,37):

$$F = \frac{(F^{\circ}_F + \sigma_F[U]) + (F^{\circ}_{UN} + \sigma_{UN}[U]) \cdot e^{-\frac{(\Delta G^{\circ}_F(H_2O) - m\cdot[U])}{RT}}}{\left(1 + e^{-\frac{(\Delta G^{\circ}_F(H_2O) - m\cdot[U])}{RT}}\right)} \quad (1)$$

Where $\Delta G^{\circ}_F(H_2O)$ is the folding free energy, m is the dependence of $\Delta G^{\circ}_F(H_2O)$ on urea concentration (kcal/M•mol), F°_F and F°_{UN} are the fluorescence signals of the folded and

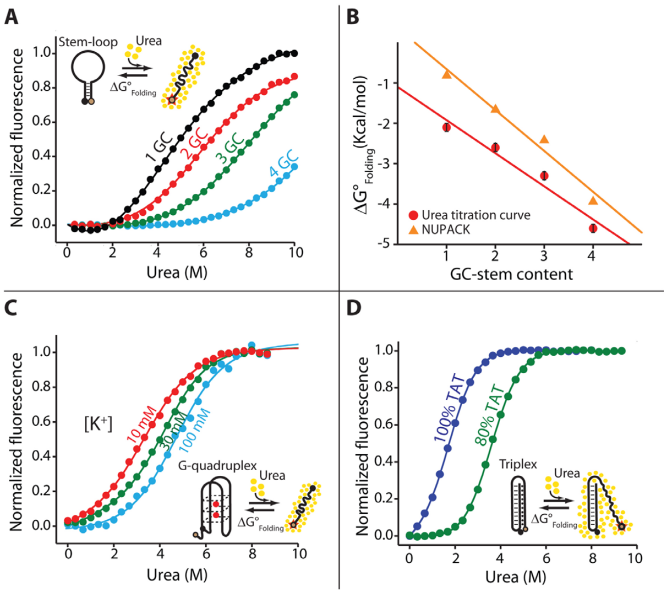

Figure 2. Determining the folding free energy of DNA unimolecular structures. (**A**) Urea titration curves of four DNA stem-loop constructs differing in their stem stability (different GC/AT content—Supplementary Figure S1). (**B**) Comparison between the experimentally and predicted (NUPACK) (15) folding free energies. (**C** and **D**) Urea titration curves of more complex DNA tertiary structures: (C) a DNA G-quadruplex (38), which is known to be specifically stabilized by K^+ ions. (D) A DNA parallel triplex structure formed by TAT versus CGC triplets (41,42). Urea titration curves were obtained in a solution of 0.1 M Tris buffer, 10 mM $MgCl_2$, pH 7.8 at 37°C for the stem-loop constructs (10 nM). For the G-quadruplex structure (20 nM) a solution of 50 mM Cs-HEPES, pH 7.5 at 25°C at different concentrations of KCl was used. For the triplex construct (50 nM) a solution of 50 mM sodium phosphate buffer, pH 7.0 at 25°C was used.

unfolded states, respectively, in absence of urea; and σ_F and σ_{UN} represent the dependence of the fluorescence signal of the folded and unfolded states, respectively, on urea concentration (23,24,36). We note that for certain unimolecular structures tested in this work some of these values have been fixed during fitting in order to improve the procedure. For example, for the σ_F value for the stem-loop constructs we used the value obtained with the variant 4GC (which shows the longest and thus the more precise initial baseline) and for the σ_{UN} value we used the value obtained from the linear extrapolation of the final portion of the curve obtained for the variant 1GC. Similarly, for the F°_{UN} value we used the value obtained by linear extrapolations of the final portion of the urea titration curves for the 1GC stem-loop. These assumptions (which are quite common in urea denaturation experiments) (23,28,37) allow to better fit the experimental values and to decrease possible errors that might arise when denaturation curves present incomplete initial or final baselines. Using these fits, we determined that the folding free energies of these stem-loop constructs range between -2.1 ± 0.1 (variant 1GC) and -4.6 ± 0.1 kcal/mol (variant 4GC) and that the average change in free energy per AT→GC substitution in the stem is -0.8 ± 0.1 kcal/mol. These values compare well with those predicted by NUPACK (15) (Figure 2B and Supplementary Table S1). The slight difference in energy observed between the predicted and experimental values (e.g. 1.3 kcal/mol for the 1GC) may likely be attributed to the interaction between the fluorophore (6-FAM) and the quencher (BHQ-1). This contribution has been already demonstrated to stabilize stem-loop structures (e.g. by 1.8 kcal/mol) (37) and it is not currently taken into account by prediction softwares (17,18).

In addition to determining the folding free energy of DNA structures, urea titration curves also allow to generate structural information through the estimation of the *m*-value, which describes the dependence of folding free energy on urea concentration (represented by the cooperative level of the urea curve). The *m*-value provides a measure of the change in solvent accessible surface area (SASA) upon unfolding and can be thus used to estimate the magnitude of the overall structural change that accompanies structure unfolding (26,28). As expected, we found that the *m*-value of all four, structurally similar, stem-loop variants remains constant (average *m*-value = 0.42 ± 0.01 kcal/M•mol) (Supplementary Table S1).

We also determined the folding free energy of more complex unimolecular DNA structures stabilized by non canonical interaction (not Watson–Crick) for which no prediction softwares are currently available. To demonstrate this, we selected a DNA G-quadruplex structure (38), which is found in many DNA aptamers and DNAzymes (39,40) and a triplex forming DNA sequence (41,42) that is often used as a pH nanosensor or nanoactuator (43,44). The urea titration curves of both these DNA tertiary structures fit well to a two-state denaturation model, Equation (1), with folding free energies of -2.6 ± 0.1 kcal/mol for the G-quadruplex (Figure 2C, at 100 mM of K^+ ions) and -2.3 ± 0.1 kcal/mol for the triplex construct (Figure 2D, 100% TAT at pH 7.0) (Supplementary Figures S2 and 4). We note here that the two-state assumption should be carefully investigated for each specific case (45). In this work, for example, we have demonstrated that the transition observed during triplex nanoswitch unfolding consists in a triplex-to-duplex transition by using a control switch lacking the triplex-forming portion (Supplementary Figure S5). For the G-quadruplex we relied on previous melting experiments performed on similar DNA sequences, which support the two-state assumption (38,45). Urea titration curves also allow to determine the stabilizing effect of potassium ions on the G-quadruplex structure (Figure 2C and Supplementary Figure S4) and of pH and base substitution on the triplex structure (Figure 2D and Supplementary Figure S2). Consistent with previous observations (38), for example, we found that the stability of the G-quadruplex increases by –0.9 kcal/mol when the potassium ions concentration is increased from 10 to 100 mM (Supplementary Figure S4). Similarly, by substituting AT interactions with CG interactions in the triplex construct sequence we were able to measure the overall contribution of C•G Hoogsteen base pairing in the folding free energy of the triplex structure and its stability in function of pH. We found that C•G Hoogsteen interaction stabilizes the triplex construct by -2.1 ± 0.4 kcal/mol at pH 6.0 and by only -0.5 ± 0.3 kcal/mol at pH 7.0 (Supplementary Figure S2). Of note, the much larger *m*-value of the triplex construct (1.08 ± 0.04 kcal/M•mol) compared to that of the G-quadruplex (0.51 ± 0.01 kcal/M•mol) and of the stem-loop (0.43 ± 0.02 kcal/M•mol) (Supplementary Figures S2 and 4) suggests that the triplex structure buries nearly twice

as much surface area upon folding than the other two structures (26,28).

The suitability of urea titration method to derive free energy values of DNA unimolecular structures is further supported by comparison with thermal melting curves obtained using the conventional Van't Hoff method (20, 38)). More specifically, the folding free energy values of the stem-loop systems (Supplementary Figure S6) obtained with thermal melting curves are in good agreement with those obtained using urea denaturation curves. Good agreement was also observed with the triplex systems (Supplementary Figure S7) although with some discrepancy with the 80% TAT switch at pH 6.0. A similar discrepancy among the results obtained with the urea denaturation curves and the thermal melting curves was also observed with the G-quadruplex systems (Supplementary Figure S8). We note here that this discrepancy might be due to the fact that the Van't Hoff analysis assumes that Enthalpy (ΔH) is independent from the temperature, which in turn means that the heat capacity change during the reaction (ΔC_p) is zero. The $\Delta C_p = 0$ hypothesis is clearly not always valid for melting of nucleic acid structures and this could account for large errors in the extrapolated ΔG° (20,38,46,47). Another potential source of the disagreement between urea and thermal denaturation measurements could also be the possible interaction between urea and ions in solution. Since it has been observed with RNA sequences that interactions of urea with monovalents ions may be important in unfolding experiments (28,48) this may be one of the reasons of the observed discrepancy.

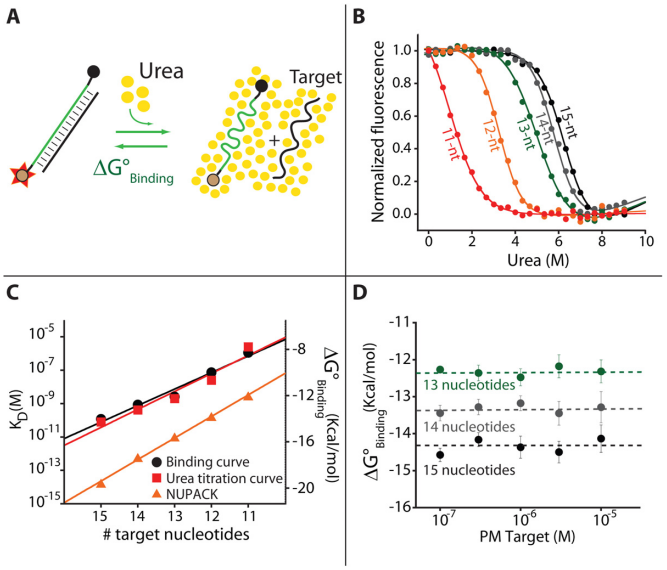

Figure 3. Determining binding free energies of DNA complexes. (**A**) Urea unfolding of DNA duplex. (**B**) Urea titration curves of five complementary DNA–DNA dimers of different length (from 11 to 15 nt—Supplementary Figure S9). (**C**) Comparison between the experimentally derived binding free energies obtained using urea titration curves (squares) and binding curves (circles) and the energies estimated by NUPACK simulation (15) (triangles) (Supplementary Table S2). (**D**) Binding free energies estimated using urea titration curves can be measured at different target concentration (Supplementary Figures S9 and 11). Dotted lines represent the average values. All urea titration and binding curves were obtained in 0.1 M Tris buffer, 0.01 M $MgCl_2$, pH 7.8 at 37°C using a fixed concentration of DNA linear probe (10 nM).

Determining binding free energies of DNA–DNA complexes

Urea titration curves can be used to precisely determine the binding free energy between complementary DNA strands (Figure 3A), a key parameter to take into account when designing, for example, DNA nanostructures that assemble using complex annealing procedures. To demonstrate this, we designed a set of complementary DNA–DNA complexes of various lengths (and thus various stabilities). Specifically, we used a fluorophore/quencher labeled 17-nt DNA strand and a set of five complementary DNA sequences (targets) with length varying from 11 to 15 nt (Supplementary Figure S9A). As shown in Figure 3B and Supplementary Figure S9B, the urea titration curves of these DNA dimers reveal a single unfolding transition, which is well fitted using a two-state unfolding model (49). Using this model, we can obtain the binding free energy of the bi-molecular systems in absence of urea, $\Delta G^\circ_B(H_2O)$, for a specific concentration of target [T_{tot}], Equation (2) (SI section 5):

$$F = \frac{[T_{tot}]\cdot(F^\circ_B + \sigma_B[U]) + (F^\circ_{NB} + \sigma_{NB}[U])\cdot e^{-\frac{(\Delta G^\circ_B(H_2O) - m\cdot[U])}{RT}}}{\left([T_{tot}] + e^{-\frac{(\Delta G^\circ_B(H_2O) - m\cdot[U])}{RT}}\right)} \quad (2)$$

Where F°_B and F°_{NB} are the fluorescence signals of the bound and not-bound states, respectively, in absence of urea; and σ_B and σ_{NB} represent the dependence of the fluorescence signal of the bound and not-bound states, respectively, on urea concentration (23,24,36). In order to facilitate fitting, we typically fixed the $\sigma_B$value for some of these denaturation curves (see SI for details). By using this model we found binding free energies between -7.9 ± 0.1 kcal/mol (11-nt target) and -14.3 ± 0.1 kcal/mol (15-nt target), which correspond to dissociation constants, K_D, of 2.5 ± 0.1 μM and 81 ± 4 pM. The K_D values determined using urea titration curves are in close agreement with those obtained through conventional binding curves (i.e. achieved by adding increasing concentration of target to a fixed concentration of the probe) (Figure 3C and Supplementary Figure S10). A clear advantage of urea titration curves over classic binding titration curves, however, is that they enable the determination of affinity constants well below the nanomolar regime (e.g. 15–nt target shows a K_D of 81 pM). In contrast, fluorescent-based binding curves are less precise for low dissociation constants (K_D) values as the titration becomes stoichiometric and it is not possible to obtain reliable information about K_D (50). Another important advantage of urea titration curves is that the binding free energy of a complex can be determined at various concentration of target thus enabling measurement of weak binding energies by driving complex association via addition of a saturated amount of target (Figure 3D and Supplementary Table S2). The results obtained with this system at different concentration of targets also support the hypothesis that the binding free energy varies linearly with the urea concentration, as previously demonstrated for protein (23,24) and RNA (26,28). We show, in fact, that both binding free energy values and *m*-values remain constant over a wide range of target concentrations (Figure 3D and Supplementary Figure S11).

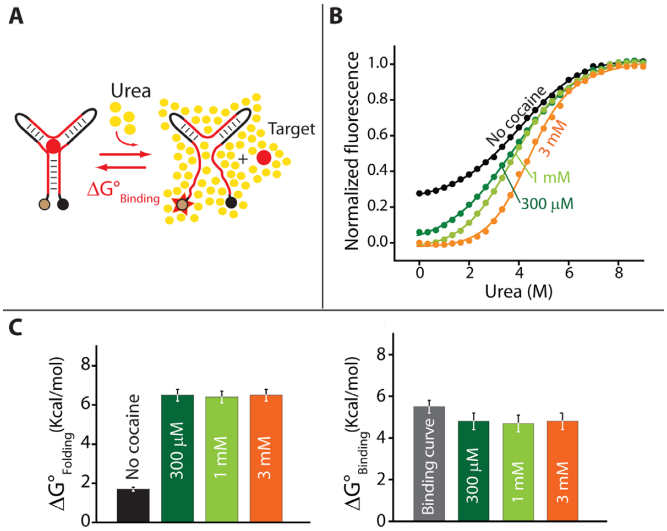

Figure 4. Determining the binding free energy of a DNA aptamer for its target. (**A**) Urea unfolding of the cocaine-binding aptamer. (**B**) Urea titration curves of the cocaine-binding aptamer in absence (black) and presence of different cocaine concentrations. (**C**) Comparison between folding and binding free energies of the cocaine-binding aptamer obtained using urea titration curves (at different concentrations of cocaine) and a classic binding curve (gray) (Supplementary Figures S12 and 13). The urea titration and binding curves were obtained in 50 mM sodium phosphate buffer, 500 mM NaCl, pH 7.0 at 25°C using 100 nM of aptamer.

Interestingly, although we find that NUPACK correctly predicts the difference in energy between our targets (e.g. for each GC addition: −1.8 kcal/mol for NUPACK versus −1.5 ± 0.2 kcal/mol for urea titration curves, Figure 3C and Supplementary Table S2), it also significantly overestimates the total binding free energy (from 3.1 to 5.1 kcal/mol) (Supplementary Table S2). The observed differences between experimental and predicted values may likely be attributed to chemical modifications (i.e. introduction of fluorophore/quencher pair) (18), multinucleotide dangles (51) or specific buffer-salt conditions (51), which are known to affect the stability of DNA–DNA complexes and that are not taken into account by prediction softwares.

Determining the binding free energy between a DNA aptamer and its target

Through the use of various selection/amplification strategies, chemists have identified a variety of DNA sequences, called aptamers, that fold or self-assemble into specific conformations that confer them binding activities to non-DNA targets (52,53). However, up to date, characterizing the binding affinity of aptamers toward their specific targets remains relatively challenging (54). Here we show that urea titration curves allow to measure the binding free energy of a DNA aptamer for its target. As a model system we employ the cocaine-binding aptamer, a well-characterized 38-nt sequence known to specifically bind cocaine and other analogues, and which undergoes a target-induced folding into a three-way junction (55). To determine the binding free energy of this aptamer for cocaine we assume that cocaine only binds the folded aptamer and measure the difference in folding free energy of the aptamer in presence and absence of cocaine. The urea titration curve of the fluorophore/quencher-labeled aptamer (Figure 4A) in absence of cocaine displays a single two-state unfolding transition which, using Equation (1), allows to estimate its folding free energy (−1.7 ± 0.1 kcal/mol)(Figure 4B and Supplementary Figure S12) (56). In the presence of saturating concentrations of cocaine (we tested 3.5 K_D, 12 K_D and 35 K_D) the urea unfolding curve shifts to higher urea concentrations, consistent with the fact that cocaine stabilizes the folded conformation (Figure 4B and Supplementary Figure S12) (57). We can estimate the binding energy of the aptamer–cocaine complex, and therefore its K_D, by simply subtracting the folding free energies estimated in absence and presence of cocaine using Equation (2) (Figure 4C). The value obtained (e.g. −4.8 ± 0.4 kcal/mol or K_D = 302 ± 25 µM when using a cocaine concentration of 300 µM) is found relatively independent of the concentration of cocaine employed and compares well with the binding free energy obtained using typical binding curve experiments (−5.5 ± 0.3 kcal/mol, K_D = 85 ± 1 µM) (Figure 4C and Supplementary Figure S13). In addition, we also found that the *m*-value is about 50% higher in presence of cocaine (0.69 versus 0.46 kcal/M•mol), suggesting that cocaine binding to the aptamer significantly reduces the access of urea to the nucleobases (Supplementary Figure S12).

Determining the binding free energy between a DNA switch and its target

Binding-induced DNA conformational switches are the basic functional units of a wide variety of nanodevices including structure-switching biosensors, molecular computers and drug delivery machines (7,11,31–35). In the vast majority of cases the conformational switches can be described by a population-shift mechanism in which target binding competes with structure switching (or structure folding) (Figure 1D). In these cases, the binding free energy between a target and a conformational molecular switch, ΔG°_B, depends on both the intrinsic affinity of the target for the binding competent conformation of the switch ($\Delta G^\circ_B{}^{int}$) and on the switching (or folding) equilibrium constant, K_F, following this relationship (37):

$$\Delta G^\circ_B = -RT\ \ln\left[\frac{1}{K_D^{int}}\left(\frac{K_F}{1+K_F}\right)\right] = \Delta G^{\circ int}_B - RT\ln\left(\frac{K_F}{1+K_F}\right) \qquad (3)$$

where, $K_D{}^{int}$ and $\Delta G^\circ_B{}^{int}$ are the dissociation constant and binding free energy between the target and binding-competent conformation of the switch and K_F (or ΔG°_F in Figure 1D) are the equilibrium constant of the switch (or its folding free energy) (Figure 1D).

Here we show how urea titration curves enable to measure binding free energies of a binding-induced DNA conformational switch using molecular beacons (31,32), a classic DNA-based switch routinely employed as a biosensor in polymerase chain reaction diagnostic tests. In this system, the thermodynamic equilibrium between a closed stem-loop (non-binding) conformation and the open (binding) conformation is shifted toward this latter in the presence of a single strand complementary to the loop sequence (Figure 5) (31,37). Here we have used the same set of four stem-loop optically-labeled constructs described in the previous

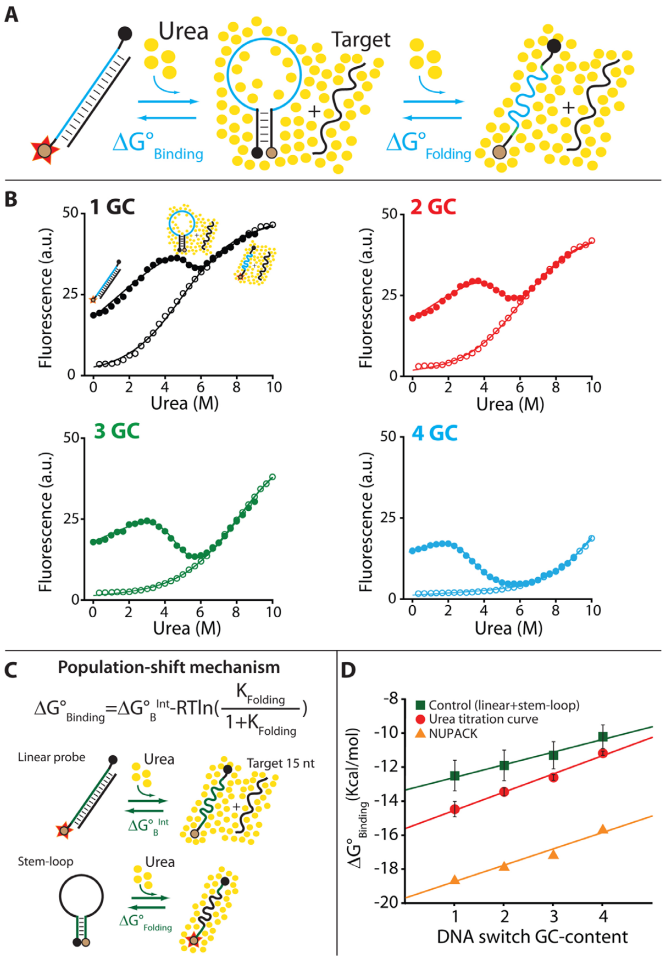

Figure 5. Determining the binding free energy between a DNA nanoswitch and its target. (**A**) Here we used as a model system a stem-loop DNA probe that recognizes a specific DNA sequence complementary to the loop sequence and, upon binding, undergoes a conformational change (stem-loop opening). (**B**) Urea titration curves of the stem-loop construct alone (empty markers) and in the presence of saturating concentrations of a DNA target (filled markers). (**C**) The population-shift mechanism correctly describes the binding between the DNA conformational switch and its target (37), so we can indirectly estimate the binding free energy between the set of four DNA switches and a 15-nt complementary target by indirectly deriving the intrinsic affinity of the binding competent conformation (K_D^{int}) and the switching-equilibrium constant (K_F) of the same stem-loop constructs in the absence of target (Supplementary Table S1). (**D**) Binding free energies obtained by urea titration curves (circles) and by NUPACK simulation (triangles) (15). Shown are also the binding free energies calculated by using the indirect method described in the text (Supplementary Figure S6C and text for details). The urea titration curves were obtained in 0.1 M Tris buffer, 0.01 M $MgCl_2$, pH 7.8 at 37°C using a fixed concentration of the relative DNA nanoswitch (10 nM).

section (Supplementary Figure S1), that display a common recognition loop domain (Supplementary Figure S14A).

The urea titration curve of these stem-loop structures at saturating concentration (1 μM) of a 15-nt target complementary to the loop domain (Figure 5B, closed symbols, and Supplementary Figure S14B) typically reveals two unfolding transitions. The first transition provides thermodynamic information about the binding free energy, ΔG°_B and represents the dissociation of the target from the switch with the switch returning into its folded conformation (of note, a significant fraction of the least stable switch 1GC remains unfolded upon target dissociation even at low urea concentration). The second transition provides thermodynamic information about the equilibrium constant of the switch, K_F (or ΔG°_F) and represents the unfolding of the molecular beacon into its open conformation. Of note, this portion of the curve precisely overlaps the urea titration curve of the stem-loop structure alone (Figure 5B, empty symbols, respectively). In order to fit this double-transition curve we have used a three-state denaturation model, which enables to estimate the binding free energy of the bimolecular system, $\Delta G^\circ_B(H_2O)$, as a function of the total target concentration $[T_{tot}]$, the stability of the stem-loop structure, $\Delta G^\circ_F(H_2O)$ and the urea concentration, Equation (4) (SI section 5):

$$F = \frac{[T_{tot}]\cdot(F^\circ_B+\sigma_B[U])+\left((F^\circ_{NB}+\sigma_{NB}[U])+(F^\circ_{UN}+\sigma_{UN})\cdot e^{-\frac{(\Delta G^\circ_F(H_2O)-m_F\cdot[U])}{RT}}\right)\cdot e^{-\frac{(\Delta G^\circ_B(H_2O)-m\cdot[U])}{RT}}}{\left([T_{tot}]+e^{\frac{(\Delta G^\circ_B(H_2O)-m\cdot[U])}{RT}}\cdot e^{-\frac{(\Delta G^\circ_F(H_2O)-m_F\cdot[U])}{RT}}+e^{-\frac{(\Delta G^\circ_B(H_2O)-m\cdot[U])}{RT}}\right)} \quad (4)$$

Where, F°_B and F°_{NB} are the fluorescence signals of the bound and not-bound (folded) states, respectively, in absence of urea; and σ_B and σ_{NB} represent the dependence of the fluorescence signal of the bound and not-bound states (folded), respectively, on urea concentration (23,24,36). Of note, F°_{UN} and σ_{UN} are the fluorescence signal in absence of urea and the dependence of the fluorescence signal on urea concentration of the unfolded state; $\Delta G^\circ_F(H_2O)$ and m_F are the folding free energy and the relative *m*-value of the stem-loop structure alone. These values can thus be easily obtained using the urea titration curves of the stem-loop structures in the absence of the target (Figure 5B, empty markers and Supplementary Table S1). The resulting fitting (Figure 5B, filled markers) thus enables to distinguish and estimate the binding free energy of the bi-molecular system, $\Delta G^\circ_B(H_2O)$, as a function of the total target concentration $[T_{tot}]$ and urea concentration, Equation (4) (SI sections 2 and 5). Using this approach we determined that the binding free energy values of our set of binding-induced DNA conformational switches for a 15-nt target range from -11.5 ± 0.1 kcal/mol (4GC-stem, more stable switch) to -13.9 ± 0.1 kcal/mol (1GC-stem, least stable switch) (Figure 5D and Supplementary Table S3). These results illustrate well how target binding competes with structure switching (or structure folding) in binding-induced conformational switches. Indeed, we found that the affinity, K_D^{obs}, of our binding-induced DNA conformational switch is inversely correlated with its switching (or folding) equilibrium constant, K_F, as described by the three-state population-shift mechanism (Supplementary Figure S15) (37).

We note that the binding free energy between the DNA switch and the 15-nt target can also be indirectly derived using two independent urea denaturation experiments and Equation (3) (Figure 5C). To do this we obtained K_D^{int} using a non-switching DNA (having the same recognition sequence of the DNA switch but lacking the switching domain, Supplementary Figures S9A and 14) in complex with the same 15-nt target employed above (Figure 5C). Similarly, we can obtain K_F using the same stem-loop constructs in the absence of target (Figures 2A and B, Supplemen-

tary Table S1). The ΔG°_{B} values obtained with this method are in relatively good agreement with those obtained from the urea titration curves of the switch-target complex and our three-state model (Figure 5D and Supplementary Table S3, within 2 kcal/mol). In contrast, we find that using NUPACK simulations and Equation (3) leads to a significant overestimation of the binding free energy by nearly 6 kcal/mol (or more than two order of magnitude in K_D variation) (Figure 5D). This clearly highlights the lack of accuracy of current DNA simulations softwares when estimating the thermodynamics of more complex nanoscale systems such as binding-induced DNA conformational switches.

DISCUSSION

Here we have demonstrated the use of urea titration experiments as a valuable tool to estimate the binding and folding free energy of various DNA-based systems. We have used a set of DNA-based nanoswitches and nanodevices that are based on simple Watson–Crick interactions or on more complex non-canonical interactions between single or multiple interacting DNA strands. More specifically, we have developed a set of equations that allow to analyze urea titration curves of different DNA secondary and tertiary structures (stem-loop, G-quadruplex, triplex structures), DNA complexes involving aptamers and binding-induced DNA switches, and to correctly estimate their relative folding and binding free energy values in presence of various ions or buffer. In addition, because urea denaturation curves also provide a measure of the surface area exposed upon unfolding, the *m*-value (or cooperativity), this approach also provides additional structural insights on the investigated DNA-based systems. Finally, we note that these thermodynamic parameters are obtained in a simple, isothermal procedure that can be performed in aqueous buffer conditions.

The use of urea titration curve to achieve structural and thermodynamic information about DNA-based or other supramolecular systems appears particularly advantageous compared to currently used methods. For example, while recently developed online softwares are able to predict with good approximation DNA–DNA interactions in different working conditions (ionic strength, DNA strand concentrations, etc.) they also present key limitations that can hinder their utility in numerous applications. These softwares, for example, are not able to correctly predict secondary and tertiary structures that contain non-canonical DNA–DNA interactions, and are not programmed to consider the effect of chemical modifications, which remain hard to predict (e.g. fluorophore, quencher, etc.). They also perform rather poorly when dealing with more complex supramolecular systems such as binding-induced DNA switches that use simple Watson–Crick based interactions (Figure 5D). Experimental methods normally employed to achieve thermodynamic information also present crucial limitations (4). Binding curve experiments, for example, typically fail to evaluate affinities (K_D) lower than nM concentrations due to the limiting effect of the concentration of the molecule in solution while urea unfolding curves enable to determined K_D as low as pM (Figure 3B). Thermal melting experiments allow the determination of various thermodynamic parameters in a simple and inexpensive fashion (20) but many buffers and optical labels are highly sensitive to temperature (51) and no structural information can be derived from melting curves. Moreover, the accurate extrapolation of thermodynamic parameters using melting curves is dependent on the assumption that enthalpy is temperature-independent ($\Delta C_p = 0$) which might lead to inaccurate results (20,51). Finally, microcalorimetry techniques as DSC (differential scanning calorimeter) and ITC (isothermal titration calorimeter) often require optimal experimental setting (20) or careful fitting procedures (21) and are only limited to specific free energies range (22).

We believe that the results described herein will pave the way toward the use of urea titration curves, and more generally, chemical denaturation experiments, as versatile tools to study the thermodynamics of DNA-based nanodevices in aqueous solutions. This approach would also greatly contribute to bridge the gap between the science displayed by naturally selected biopolymers (which are much more advanced that human-made chemistry) and the one displayed by modern nanotechnology. In the last thirty years, for example, urea titration has revealed the thermodynamics basis of many highly complex biochemical mechanisms (23–28). We believe that urea denaturation methods may thus be exploited with similar success to study and optimize nanoscale systems designed by human that use similar functional groups than the one displayed on biopolymers surfaces.

SUPPLEMENTARY DATA

Supplementary Data are available at NAR Online.

ACKNOWLEDGEMENTS

A.I, F.R., A.V.B conceived and designed the project. A.I. carried out the experimental works. A.I, F.R., A.V.B wrote the paper. All authors read and approved the final manuscript.

FUNDING

Associazione Italiana per la Ricerca sul Cancro, AIRC [14420 to F.R.]; European Research Council (ERC) [336493 to F.R.]; National Sciences and Engineering Research Council of Canada [2014–06403]; Funding for open access charge: ERC Starting Grant [336493].
Conflict of interest statement. None declared.

REFERENCES

1. Chen,Y.-J., Groves,B., Muscat,R.A. and Seelig,G. (2015) DNA nanotechnology from the test tube to the cell. *Nat. Nanotechnol.*, **10**, 748–760.
2. Langecker,M., Arnaut,V., Martin,T.G., List,J., Renner,S., Mayer,M., Dietz,H. and Simmel,F.C. (2012) Synthetic lipid membrane channels formed by designed DNA nanostructures. *Science*, **338**, 932–936.
3. Kuzyk,A., Schreiber,R., Fan,Z., Pardatscher,G., Roller,E.-M., Högele,A., Simmel,F.C., Govorov,A.O. and Liedl,T. (2012) DNA-based self-assembly of chiral plasmonic nanostructures with tailored optical response. *Nature*, **483**, 311–314.
4. Lau,K. L. and Sleiman,H. F. (2016) Minimalist approach to complexity: templating the assembly of DNA tile structures with sequentially grown input strands. *ACS Nano*, **10**, 6542–6551.

5. Andersen,E.S., Dong,M., Nielsen,M.M., Jahn,K., Subramani,R., Mamdouh,W., Golas,M.M., Sander,B., Stark,H., Oliveira,C.L.P. *et al.* (2009) Self-assembly of a nanoscale DNA box with a controllable lid. *Nature*, **459**, 73–76.
6. Modi,S., Swetha,M.G., Goswami,D., Gupta,G.D., Mayor,S. and Krishnan,Y. (2009) A DNA nanomachine that maps spatial and temporal pH changes inside living cells. *Nat. Nanotechnol.*, **4**, 325–330.
7. Lu,C.-H., Willner,B. and Willner,I. (2013) DNA nanotechnology: from sensing and DNA machines to drug-delivery systems. *ACS Nano*, **7**, 8320–8332.
8. Elbaz,J., Lioubashevski,O., Wang,F., Remacle,F., Levine,R.D. and Willner,I. (2010) DNA computing circuits using libraries of DNAzyme subunits. *Nat. Nanotechnol.*, **5**, 417–422.
9. Genot,A.J., Bath,J. and Turberfield,A.J. (2011) Reversible logic circuits made of DNA. *J. Am. Chem. Soc.*, **133**, 20080–20083.
10. Wickham,S.F.J., Bath,J., Katsuda,Y., Endo,M., Hidaka,K., Sugiyama,H. and Turberfield,A.J.A. (2012) DNA-based molecular motor that can navigate a network of tracks. *Nat. Nanotechnol.*, **7**, 169–173.
11. Douglas,S.M., Bachelet,I. and Church,G.M. (2012) A logic-gated nanorobot for targeted transport of molecular payloads. *Science*, **335**, 831–834.
12. Liu,M., Fu,J., Hejesen,C., Yang,Y., Woodbury,N.W., Gothelf,K., Liu,Y. and Yan,H. (2013) A DNA tweezer-actuated enzyme nanoreactor. *Nat. Commun.*, **4**, 2127.
13. Freeman,R., Sharon,E., Tel-Vered,R. and Willner,I. (2009) Supramolecular cocaine-aptamer complexes activate biocatalytic cascades. *J. Am. Chem. Soc.*, **131**, 5028–5029.
14. Zuker,M. (2003) Mfold web server for nucleic acid folding and hybridization prediction. *Nucleic Acids Res.*, **31**, 3406–3415.
15. Zadeh,J.N., Steenberg,C.D., Bois,J.S., Wolfe,B.R., Pierce,M.B., Khan,A.R., Dirks,R.M. and Pierce,N.A. (2011) NUPACK: analysis and design of nucleic acid systems. *J. Comput. Chem.*, **32**, 170–173.
16. Owczarzy,R., Tataurov,A.V., Wu,Y., Manthey,J.A., McQuisten,K.A., Almabrazi,H.G., Pedersen,K.F., Lin,Y., Garretson,J., McEntaggart,N.O. *et al.* (2008) IDT SciTools: a suite for analysis and design of nucleic acid oligomers. *Nucleic Acids Res.*, **36**, W163–W169.
17. Marras,S.A., Kramer,F.R. and Tyagi,S. (2002) Efficiencies of fluorescence resonance energy transfer and contact-mediated quenching in oligonucleotide probes. *Nucleic Acids Res.*, **30**, e122.
18. Moreira,B.G., You,Y., Behlke,M.A. and Owczarzy,R. (2005) Effects of fluorescent dyes, quenchers, and dangling ends on DNA duplex stability. *Biochem. Biophys. Res. Commun.*, **327**, 473–484.
19. Wolk,S.K., Shoemaker,R.K., Mayfield,W.S., Mestdagh,A.L. and Janjic,N. (2015) Influence of 5-N-carboxamide modifications on the thermodynamic stability of oligonucleotides. *Nucleic Acids Res.*, **43**, 9107–9122.
20. Mergny,J.-L. and Lacroix,L. (2003) Analysis of thermal melting curves. *Oligonucleotides*, **13**, 515–537.
21. Chaires,J.B. (2008) Calorimetry and thermodynamics in drug design. *Annu. Rev. Biophys.*, **37**, 135–151.
22. Cooper,A., Johnson,C.M., Lakey,J.H. and Nöllmann,M. (2001) Heat does not come in different colours: entropy-enthalpy compensation, free energy windows, quantum confinement, pressure perturbation calorimetry, solvation and the multiple causes of heat capacity effects in biomolecular interactions. *Biophys. Chem.*, **93**, 215–230.
23. Pace,C.N., Grimsley,G.R. and Scholtz,J.M. (2008) Denaturation of proteins by urea and guanidine hydrochloride. In: Buchner,J and Kiefhaber,T, (eds). *Protein Folding Handbook*. John Wiley & Sons, Inc., pp. 45–69.
24. Maxwell,K.L., Wildes,D., Zarrine-Afsar,A., De Los Rios,M.A., Brown,A.G., Friel,C.T., Hedberg,L., Horng,J.-C., Bona,D., Miller,E.J. *et al.* (2005) Protein folding: defining a "standard" set of experimental conditions and a preliminary kinetic data set of two-state proteins. *Protein Sci.*, **14**, 602–616.
25. Neri,D., Billeter,M., Wider,G. and Wüthrich,K. (1992) NMR determination of residual structure in a urea-denatured protein, the 434-repressor. *Science*, **257**, 1559–1563.
26. Shelton,V.M., Sosnick,T.R. and Pan,T. (1999) Applicability of urea in the thermodynamic analysis of secondary and tertiary RNA folding. *Biochemistry*, **38**, 16831–16839.
27. Fang,X.-W., Pan,T. and Sosnick,T.R. (1999) Mg^{2+}-dependent folding of a large ribozyme without kinetic traps. *Nat. Struct. Biol.*, **6**, 1091–1095.
28. Lambert,D. and Draper,D.E. (2012) Denaturation of RNA secondary and tertiary structure by urea: simple unfolded state models and free energy parameters account for measured m–values. *Biochemistry*, **51**, 9014–9026.
29. Jungmann,R., Liedl,T., Sobey,T.L., Shih,W. and Simmel,F.C. (2008) Isothermal assembly of DNA origami structures using denaturing agents. *J. Am. Chem. Soc.*, **130**, 10062–10063.
30. Zhang,Z., Song,J., Besenbacher,F., Dong,M. and Gothelf,K.V. (2013) Self-assembly of DNA origami and single-stranded tile structures at room temperature. *Angew. Chem. Int. Ed.*, **52**, 9219–9223.
31. Tyagi,S., Bratu,D.P. and Kramer,F.R. (1998) Multicolor molecular beacons for allele discrimination. *Nat. Biotechnol.*, **16**, 49–53.
32. Fan,C., Plaxco,K.W. and Heeger,A.J. (2003) Electrochemical interrogation of conformational changes as a reagentless method for the sequence-specific detection of DNA. *Proc. Natl. Acad. Sci. U.S.A.*, **100**, 9134–9137.
33. Juul,S., Iacovelli,F., Falconi,M., Kragh,S.L., Christensen,B., Frøhlich,R., Franch,O., Kristoffersen,E.L., Stougaard,M., Leong,K.W. *et al.* (2013) Temperature-controlled encapsulation and release of an active enzyme in the cavity of a self-assembled DNA nanocage. *ACS Nano*, **7**, 9724–9734.
34. Porchetta,A., Idili,A., Vallée-Bélisle,A. and Ricci,F. (2015) General strategy to introduce pH-induced allostery in DNA-based receptors to achieve controlled release of ligands. *Nano Lett.*, **15**, 4467–4471.
35. Green,A.A., Silver,P.A., Collins,J.J. and Yin,P. (2014) Toehold switches: de-novo-designed regulators of gene expression. *Cell*, **159**, 925–939.
36. Santoro,M.M. and Bolen,D.W. (1988) Unfolding free energy changes determined by the linear extrapolation method. 1. Unfolding of phenylmethanesulfonyl α-chymotrypsin using different denaturants. *Biochemistry*, **27**, 8063–8068.
37. Vallée-Bélisle,A., Ricci,F. and Plaxco,K.W. (2009) Thermodynamic basis for the optimization of binding-induced biomolecular switches and structure-switching biosensors. *Proc. Natl. Acad. Sci. U.S.A.*, **106**, 13802–13807.
38. Lane,A.N., Chaires,J.B., Gray,R.D. and Trent,J.O. (2008) Stability and kinetics of G-quadruplex structures. *Nucleic Acids Res.*, **36**, 5482–5515.
39. Tucker,W.O., Shum,K.T. and Tanner,J.A. (2012) G-quadruplex DNA aptamers and their ligands: structure, function and application. *Curr. Pharm. Des.*, **18**, 2014–2026.
40. Golub,E., Freeman,R. and Willner,I. (2011) A hemin/G-quadruplex acts as an NADH oxidase and NADH peroxidase mimicking DNAzyme. *Angew. Chem. Int. Ed.*, **50**, 11710–11714.
41. Sklenar,V. and Feigon,J. (1990) Formation of a stable triplex from a single DNA strand. *Nature*, **345**, 836–838.
42. Häner,R. and Dervan,P.B. (1990) Single-strand DNA triple-helix formation. *Biochemistry*, **29**, 9761–9765.
43. Chen,Y., Lee,S.-H. and Mao,C. (2004) A DNA nanomachine based on a duplex-triplex transition. *Angew. Chem. Int. Ed.*, **43**, 5335–5338.
44. Idili,A., Vallée-Bélisle,A. and Ricci,F. (2014) Programmable pH-triggered DNA nanoswitches. *J. Am. Chem. Soc.*, **136**, 5836–5839.
45. Rachwal,P.A. and Fox,K.R. (2007) Quadruplex melting. *Methods*, **43**, 291–301.
46. Mikulecky,P.J. and Feig,A.L. (2006) Heat capacity changes associated with nucleic acid folding. *Biopolymers*, **82**, 35–58.
47. Kamiya,M., Torigoe,H., Shindo,H. and Sarai,A. (1996) Temperature dependence and sequence specificity of DNA triplex formation: an analysis using isothermal titration calorimetry. *J. Am. Chem. Soc.*, **118**, 4532–4538.
48. Guinn,E.J., Pegram,L.M., Capp,M.W., Pollock,M.N. and Record,M.T. Jr (2011) Quantifying why urea is a protein denaturant, whereas glycine betaine is a protein stabilizer. *Proc. Natl. Acad. Sci. U.S.A.*, **108**, 16932–16937.
49. Idili,A., Plaxco,K.W., Vallée-Bélisle,A. and Ricci,F. (2013) Thermodynamic basis for engineering high-affinity, high-specificity binding-induced DNA Clamp Nanoswitches. *ACS Nano*, **7**, 10863–10869.
50. Van De Weert,M. and Stella,L. (2011) Fluorescence quenching and ligand binding: a critical discussion of a popular methodology. *J. Mol. Struct.*, **998**, 145–150.

51. Wang,C., Bae,J.H. and Zhang,D.Y. (2016) Native characterization of nucleic acid motif thermodynamics via non-covalent catalysis. *Nat. Commun.*, **7**, 10319.
52. Ellington,A.D. and Szostak,J.W. (1990) In vitro selection of RNA molecules that bind specific ligands. *Nature*, **346**, 818–822.
53. Tuerk,C. and Gold,L. (1990) Systematic evolution of ligands by exponential enrichment: RNA ligands to bacteriophage T4 DNA polymerase. *Science*, **249**, 505–510.
54. Chang,A.L., McKeague,M., Liang,J.C. and Smolke,C.D. (2014) Kinetic and equilibrium binding characterization of aptamers to small molecules using a label-free, sensitive, and scalable platform. *Anal. Chem.*, **86**, 3273–3278.
55. Stojanovic,M.N., de Prada,P. and Landry,D.W. (2001) Aptamer-based folding fluorescent sensor for cocaine. *J. Am. Chem. Soc.*, **123**, 4928–4931.
56. Lawrence,C., Vallée-Bélisle,A., Pfeil,S.H., De Mornay,D., Lipman,E.A. and Plaxco,K.W. (2014) A comparison of the folding kinetics of a small, artificially selected DNA aptamer with those of equivalently simple naturally occurring proteins. *Prot. Sci.*, **23**, 56–66.
57. Schön,A., Brown,R.K., Hutchins,B.M. and Freire,E. (2013) Ligand binding analysis and screening by chemical denaturation shift. *Anal. Biochem.*, **443**, 52–57.